Air-gap Flux Density Distribution of Small Induction Motor

Air-gap Flux Density Distribution of Small Induction Motor

Takemitsu ISHIZAKI*, Tsutomu TOKUDA* and Sadao ISHIKAWA*

(Received June 29, 1963)

Remarkably increasing in their range of use, small induction motors are now strictly required to reduce their vibration and noise. Though there are many causes of the vibration and noise, harmonic fluxes at the air-gap can be considered as one of the most important causes.

This paper deals with the air-gap flux density distribution of small induction motors which are used for electric fan. The harmonic fluxes, introduced by stator and rotor windings in open slots, are multiplied by the rotor current. Moreover, mechanical dis-symmetries which are due to the inevitable clearance and tolerance incident to the mass production of motor, exert vicious influences upon the flux density distribution at the air-gap.

1. Introduction

The small single-phase induction motor has recently come to be widely used in the household and office appliances, whose noise is particularly objectionable. It has become one of the most important factors in designing motor to minimize the noise as well as vibration. There are several papers[1)2)3)] on the studies of noise and vibration in the induction motor. Very few of them, however, give clear cut view on the relation of phenomena with theoretical explanation and very little is discussed about quantitative materials.

The motor noise, composed of so many delicate phenomena in itself, may take place in most occasions with relation to a number of factors overlapped to each other, but taking a view of its cause, it may roughly be divided into the two categories, namely magnetic and mechanical ones. The magnetic noise is generated by the vibrations of iron cores due to higher harmonics in the air-gap flux distribution.

As the first step to investigate fundamentally the magnetic noise in induction motor, measurements of the air-gap flux density distribution were carried out. Motors, dealt with in this paper, are 4-pole condenser motors which are commonly used in the electric fan. The air-gap flux density, including the ripples caused by the slot openings of stator and rotor, is more distorted by the influence of rotor current. The mechanical dissymmetries, such as eccentric rotor and offset stator etc., also exert vicious influences upon the flux distribution.

2. Measurement and sample

2-1. Measurement. A narrow search coil, which runs parallel with the rotor shaft as shown in Fig. 1, is pasted on the surface of the rotor. Then the rotor is set in the stator, and one of the two-phase stator windings is excited by the a-c current, but

* Department of Electrical Engineering, College of Engineering.

another winding is not excited. The flux, which interlinks the search coil, can be considered to be a sinusoidal function of the time, because it is excited by the a-c sinusoidal current. Also, the flux varies with the space position of the search coil.

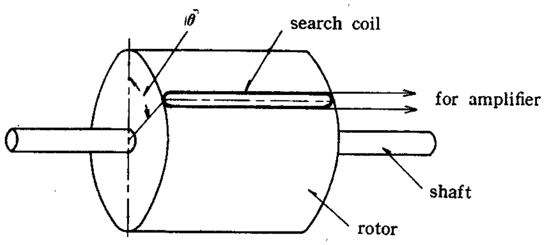

Fig. 1. Measurement of air-gap flux density.

If the width of the search coil is sufficiently narrow, it can be easily considered that the flux density at the center of the coil width is uniformly distributed over the coil surface. Then the flux ϕ_θ, which interlinks the search coil at space angle θ, can be written as the following equation,

$$\phi_\theta = dlB_\theta \sin 2\pi ft \qquad (1)$$

where B_θ; Maximum flux density at the center of the search coil (Wb/mm^2)
d; width of the search coil (mm)
l; length of the search coil (mm)
f; a-c line frequency (cps)
t; time (s)

The average value of electromotive force, induced in the coil at the angle θ, can be expressed as follows

$$E_\theta = 4N_s f dlB_\theta \qquad (2)$$

Where N_s; number of turns of the search coil.

From eq. (2), it can be easily seen that the flux density at θ is directly proportional to the emf induced in the coil. Accordingly, the distribution of flux density at the air-gap can be plotted by the measurement of emf induced in the coil.

The terminals of the search coil are connected to the slip rings which are mounted on the rotor shaft. The emf induced in the coil is led to an amplifier by the aids of slip rings and brushes. The rotor (i.e. search coil) is rotated slowly, such as 1/2 rpm, by the Warren motor. After the emf induced in the coil is amplified and rectified, it is recorded by the pen writing oscillograph. The block diagram of the measuring method is shown in Fig. 2. The plotted wave forms on the oscillogram signify the average value of the emf induced in the search coil according to the rotation of the rotor.

Fig. 2. Blook diagram of measuring method.

Since the flux density is proportional to the emf induced in the search coil, as mentioned above, the distributions of air-gap flux density around the all inside periphery of the stator, are expressed by the oscillograms per rotor revolution.

The number of turns and dimensions of the search coil, employed for the test, are as follows:

$N_s=5$, $d=1\,mm$, diameter of coil wire$=0.05\,mm$ (for all samples),

$l=20\,mm$ (for samples I, II, III), $l=27\,mm$ (for sample IV)

2-2. Sample. Four motors, employed for test, are capacitor type fan motors manufactured by different makers respectively. Each motor has 4-poles, 2-phases and 8-coils, and therefore the number of coil per phase per pole is one. The samples I, II and III are driving-motors for 30-*cm* fan, and the sample IV is the one for 40-*cm* fan.

(1) Rotor. Aluminum die-cast rotors with open slots are used in the sample motors. As the rotor bars are skewed, they are not parallel to the axis of the shaft. The dimensions of rotor of the sample motors are shown in Table I.

(2) Stator. The slots of the stator are of the open type, and not skewed. Table II shows the dimensions of the stator.

Table I. Dimensions of rotor.

No. of sample	Outside diameter (*mm*)	Width of slot (*mm*)	Width of tooth (*mm*)	Skew pitch	No. of slot
I	41.2	0.8	6.8	1.8	17
II	45.2	0.8	5.6	1.4	22
III	41.2	0.8	6.8	1.5	17
IV	39.2	0.8	6.4	1.0	17

Table II. Dimensions of stator.

No. of sample	Inside diameter (*mm*)	Length of stack (*mm*)	Width of slot (*mm*)	Width of tooth (*mm*)	No. of slot
I	42	20	3.5	13.1	8
II	46	22	3.0	15.1	8
III	42	20	3.5	13.0	8
IV	40	27	2.5	7.0/3.9	16

3. Experimental result

A single-phase winding SW_1 of stator is excited by the a-c line through the resistance R and the other winding SW_2 is not excited, as shown in Fig. 3. The terminal voltage of SW_1 is reduced to less than one half of rated voltage of the motor, for its core is not saturated. Therefore the sinusoidal current will flow through the winding SW_1. In this case, the air-gap flux is produced by the stator current in SW_1, and it is affected by the rotor current which is induced by the alternating air-gap flux.

If it is necessary to measure the air-gap flux which is not influenced by rotor current, the end rings of the rotor must be cut off. The measurements were carried out in the following two cases; the rotor with end rings and without ones.

3-1. Rotor with end rings. Fig. 4 shows the oscillograms of the search coil emf for one rotation of the rotor. They give the average values of a-c emf induced in the search coil, which are proportional to the flux density, but don't give the direction of the flux density. The magnetic poles in the stator, in which only one of the two-phase windings is excited, are such arranged that the north and south poles are alternately positioned. Therefore the air-gap flux distribution with reference to conductors, through which the exciting current flows, can be rewritten from the oscillograms in Fig. 4. The examples of the results are shown in Fig. 5 for the sample I and Fig. 6 for the sample IV.

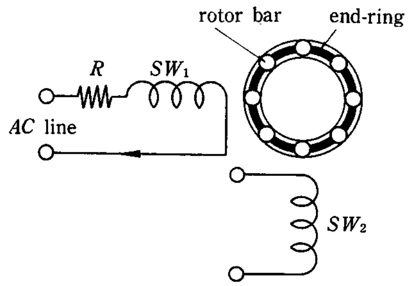

Fig. 3. Excitation by a single-phase winding.

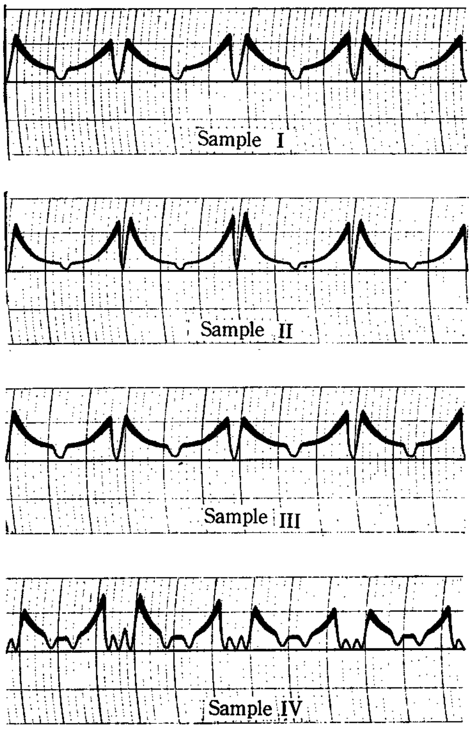

Fig. 4. Oscillograms of search coil emf distribution over one revolution.

In Figs. 5 and 6, X-axis represents the electrical angle x, which is twice the space

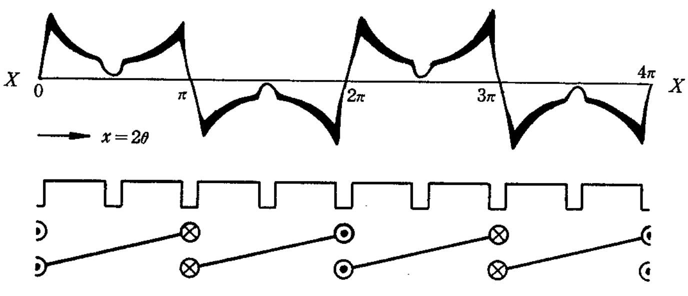

Fig. 5. Air-gap flux density distribution with reference to conductors and slots arrangement for sample I. (Rotor with endrings)

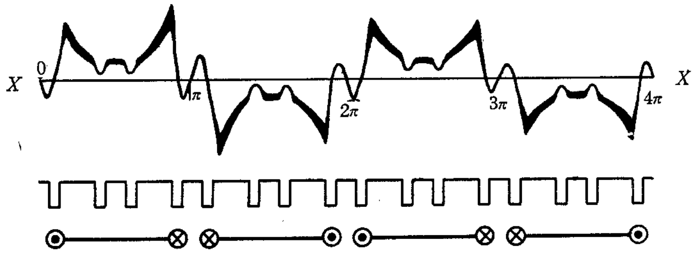

Fig. 6. Air-gap flux density distribution with reference to conductors and slots arrangement in sample IV. (Rotor with end rings)

angle θ. The flux density distribution curves per pole pitch are not identical to each other, as shown in Fig. 5 or 6. The dissymmetry of the flux curves may be due to irregularities of air-gap length. As each coil, composing a single-phase winding, is of the same type, the wave forms of mmf per pole should be identical. By the mechanical dissymmetries which are due to inevitable clearance and tolerance incident to the mass production of motor, the length of the air-gap varies with space angle θ (i.e. x). Therefore the distribution curves of the air-gap flux density are distorted.

In Fig. 4, each oscillogram for samples I, II, III and IV has eight peaks of emf (i.e. flux density) over one revolution. However the values of the peak emf in each sample are different from each other. The period of variation of peak value is a cycle per revolution. It may be considered that the rotor is not correctly set at the center of the stator. Then, the air-gap length varies with the rotation of the rotor, and the period of the variation of the air-gap length becomes also a cycle per revolution. The value of the deviation between the center of the rotor and that of the stator may be estimated from the variation rate ε in flux density over the one revolution, and ε can be represented as the following equation.

$$\varepsilon=\frac{(B_p)_{max}-(B_p)_{min}}{(B_p)_{max}+(B_p)_{min}} \tag{3}$$

where $(B_p)_{max}$: maximum value of flux density at peak in one revolution.

$(B_p)_{min}$: minimum value of flux density at peak in one revolution.

The values of ε for each sample are shown in Table III.

Table III. Values of ε.

No. of sample	I	II	III	IV
ε	0.127	0.133	0.163	0.153

3-2. Rotor without end rings. To investigate the influence of the rotor current upon the air-gap flux distribution, an experiment has been carried out for samples I and IV, in which the rotor end rings were cut off. In this case, the current can not flow througn the rotor bars, and the air-gap flux is produced only by the current of the stator winding. Thus, the air-gap flux density distributions with reference to conductors and slots arrangement, become as shown in Figs. 7 and 8 for samples I and IV respectively.

The variation rate ε in the flux density over the one revolution can be calculated from Figs. 7 and 8. The values of ε are as follows

$\varepsilon=0.125$ for sample I

$\varepsilon=0.150$ for sample IV

They are nearly equal to the values of ε indicated by Table III, respectively.

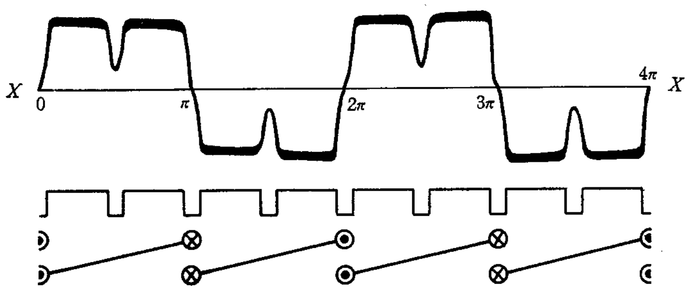

Fig. 7. Air-gap flux density distribution with reference to conductors and slots arrangement for sample I. (Rotor without end rings)

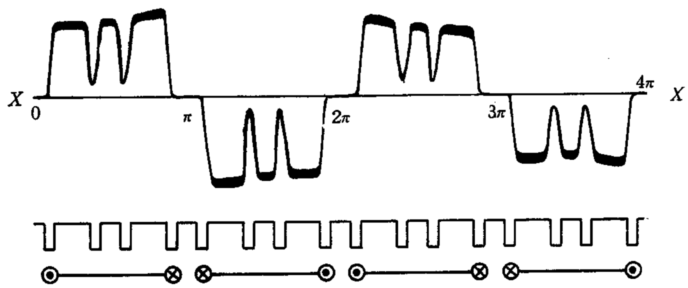

Fig. 8. Air-gap flux density distribution with reference to conductors and slots arrangement for sample IV. (Rotor without end rings)

4. Calculation and discussion

4-1. Harmonic calculation. Now, the measured air-gap flux density distribution shall be examined and analyzed. The curves of the flux distribution can be expressed by Fourier series. To make the calculation more simple, the mechanical dissymmetries should be eliminated. Then the flux density distribution curves per pole pitch become identical to each other. The flux density $B(x+\pi)$ at a point $(x+\pi)$ is equal to the flux density at a point x and has opposite sign, i.e.

$$B(x+\pi)=-B(x) \tag{4}$$

It may be considered that the each wave is symmetric about the center of the wave. Hence, for $x=0\sim\pi$

$$B(\pi - x) = B(x) \tag{5}$$

Applying eqs. (4) and (5) for measured curves of flux distribution, the curves will be represented by simple periodical wave. The simplified wave forms are shown in Fig. 9 for sample I and Fig. 10 for sample IV.

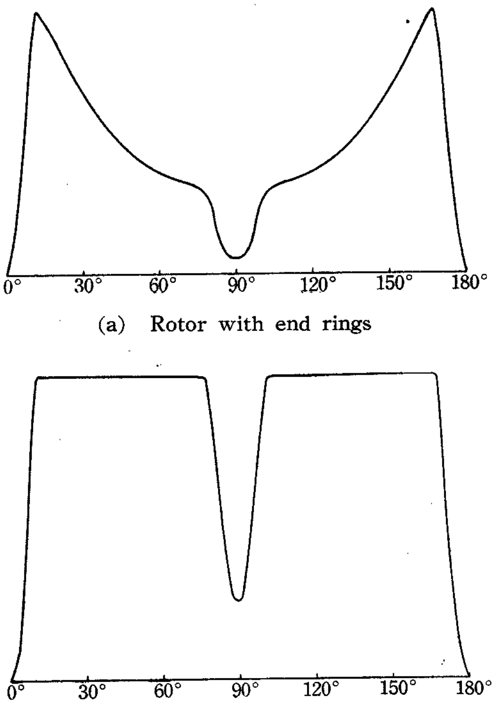

(a) Rotor with end rings

(b) Rotor without end rings

Fig. 9. Simplified flux density distribution of air-gap per pole pitch for sample I.

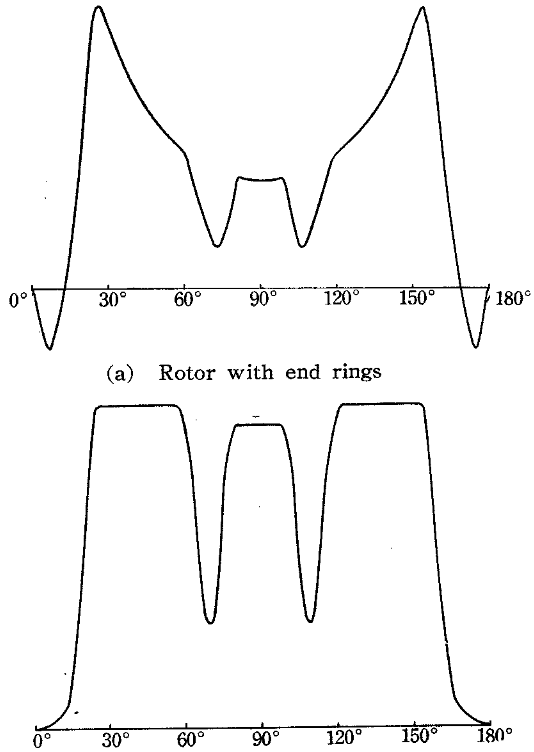

(a) Rotor with end rings

(b) Rotor without end rings

Fig. 10. Simplified flux density distribution of air-gap per pole pitch for sample IV.

From eqs. (4) and (5), Fouries series which represent the wave forms in Figs. 9 and 10, can not contain the even harmonics or the cosine terms. Hence, the flux density $B(x)$ can be written as following,

$$\begin{aligned} B(x) &= B_1 \sin x + B_3 \sin 3x + B_5 \sin 5x + \cdots\cdots \\ &= B_1\left(\sin x + \frac{B_3}{B_1}\sin 3x + \frac{B_5}{B_1}\sin 5x + \cdots\cdots\right) \end{aligned} \tag{6}$$

The ratios of harmonic flux densities to fundamental one, B_3/B_1, B_5/B_1, B_7/B_1 ……, can be calculated from the wave forms. The results of the calculation are shown in Table IV for sample I and Table V for sample IV.

The rectangular mmf is generally set up by a single coil, no matter whether the coil has full pitch winding or short pitch one. And since the usual calculations[4] are carried out under some assumptions that the flux density wave would have the identical shape

Table IV. Harmonic content of air-gap flux density distribution and mmf for sample I. (Ratio: harmonic/fundamental)

Degree of harmonics	Flux density		MMF (Rectangular wave)
	Rotor with end rings	Rotor without end rings	
3	0.878	0.442	0.333
5	0.529	0.091	0.200
7	0.335	0.189	0.143
9	0.083	−0.012	0.111
11	0.096	−0.278	0.091

Table V. Harmonic content of air-gap flux density distribution and mmf for sample IV. (Ratio: harmonic/fundamental)

Degree of harmonics	Flux density		MMF Rectangular wave
	Rotor with end rings	Rotor without end rings	
3	0.587	0.262	0.206
5	−0.065	−0.024	0.000
7	−0.404	−0.060	−0.088
9	−0.200	0.030	−0.111
11	−0.315	−0.166	−0.091

with the mmf wave, harmonic contents of rectanglar mmf wave, are also shown in these tables for ready comparisons.

4-2. Discussion. Following facts can be clarified from the above results of the harmonic calculations.

(1) Slot openings in the stator and rotor tend to exaggerate the effects of certain harmonics. Its example can be shown in Table IV, where the third harmonic for rotor without end rings becomes 0.442, in comparison with the value of 0.333 for mmf.

(2) Induced currents, flowing in the rotor bars, increase the harmonics particularly. This fact is clearly shown by Tables IV and V.

Though it has been generally considered that harmonics in the flux wave are damped appreciably by the rotor currents and the flux distribution at the air-gap approaches to the sinusoidal wave more than mmf wave, the above results for the sample motors show the opposite tendency which can give the better explanation to the generation of the noise and vibration of the motor.

There is, moreover, such phenomenon that irregularities of the gap length, caused by mechanical dissymmetries which are eliminated in the above calculations, exert vicious influences upon the flux distribution. The discrepancy of the wave form per pole pitch from each other is surely promoted by this phenomenon on which the studies are continued by the authors.

5. Conclusion

Through the actual measurements of the distributions of the air-gap flux density and the analyses on the experimental results, the harmonic content in the flux disttribution, which is one of the most important causes of noise and vibration, can be quantitatively obtained for the small induction motor. It is also clarified that the secondary current induced in the rotor bars is a serious factor on the distortions contained in the flux density distribution. It is furthermore worthy of special emphassis that the mechanical dissymmetries exert vicious influences upon the flux density distribution.

References

1) D. F. Muster and G. L. Wolfert; AIEE Transactions **74,** 1365 (1956).
2) L. W. Magyar; AIEE Power Apparatus and Systems **81,** (April 1959).
3) N. Abe and K. Maruyama; Toshiba Review **14,** 915 (1959).
4) C. G. Veinott; Theory and Design of Small Induction Motor (book), 272, McGrow-Hill co. (1959).